Numerical Predictions of Three Parallel Jets Interaction

Nassira Nouali and Amina Mataoui
Theoretical and applied laboratory of fluid mechanics Faculty of physics
University of science and Technology of Algiers - USTHB, Algiers, Algeria
Emails: nouali_nassira@yahoo.fr; mataoui_amina@yahoo.fr

Received date: 12/1/2013; Accepted date: 6/21/2014

ABSTRACT

This work is about the interaction of three parallel non-ventilated turbulent slot jets. The central jet is set symmetrically between two identical lateral heated jets. There are so many applications of this flow configuration in engineering such as gas turbine airfoils, heating or cooling surfaces, combustion and mixing flow. Computations are achieved by finite volume method. The numerical predictions confirm the three types of flow patterns given by the available flow visualization. Furthermore, a fourth type of flow pattern is found in this paper. For a given distance between two neighboring jets of 11 times the nozzle thickness ($D_0 = 11a$), the effects of the velocity ratio on the dynamical and thermal flow fields are examined. Therefore, the contours of the streamlines, vorticity, pressure, kenetic turbulence energy and isotherms for several velocity ratios ($0.3 \leq \lambda \leq 15$), are discussed in this paper. Several temperature gaps ($10°C \leq \Delta T \leq 50°C$) between the two neighboring jets are considered. Both centerline and crosswise profiles of the averaged velocity and temperature are found similar for several temperature gaps at each velocity ratio. In the developed region, a comparison between the available data of the single free jet and those of the three jets is carried out in order to evidence the effect of the presence of the two side jets on the mixing phenomenon and heat transfer. It was found that the addition of the side jets increases the rate of decrease of the average velocity along the central jet axis for the flow of type A and decreases the rate of decrease for the other types of flow. The effect of various types of flow on the spreading decrease of the velocity and the temperature in the fully developed flow region is also investigated. The diffusion of temperature depends strongly on velocity ratio (λ).

Key Words: Triple jet; free plane jet; turbulence; finite volume; mixing flow; stagnation point; heat transfer

1. INTRODUCTION

Since many decades, parallel turbulent multijet are investigated experimentally and numerically by many researchers: Tanaka and Nakata [1], Tanaka [2] and [3] , Krothapalli et al. [4], Raghunathan and Reid [5], Elbanna et al. [6], Jung and Yoo [7], Nasr and Lai [8], Kimura et al. [9], Tokuhiro and Kimura [10], Yamamoto and Hishida [11], Buddhika [12]. The mixing by jets is used in several application of fluid mechanic, such as the burners, the ejectors of VTOL and STOL aircrafts, the fluidics, and the injection systems. In multijet studies, the mutual influence of the adjacent jets on each other requires clear understanding and hence three jets interaction become interesting. To investigate such interaction is quite complex because each jet is subjected to the compression and expansion of its shear layer. In view of these complexities, it is recommended to control the mixing between the jets and the entrainment of the surrounding flow. The aligned jets are also studied by other authors. The works of Salentey [13] and Lesieur [14] have examined the configuration of three aligned injectors: a central jet of natural gas and two lateral jets of pure oxygen. These works are carried on the dynamic and scalar fields as well as the behavior of oxy-flame depending on the dynamical and geometrical parameters of the burner study. The measurements made, for several velocities and distances between the jets, allowed to point out the influence of these parameters on the stabilization of oxy-flame as well as modifying the topology and the characteristics of the flows. In the case of flow resulting from jets and whatever the geometry of the injectors, it is possible to describe the overall flow through the three regions found previously in Refs. [1], [15] and [16]:

– The Combining zone is the region of the flow where the jets are not yet in complete interaction. for the non-ventilated jets (where the space between the nozzles is confined by a wall), this zone is characterized by vortices and it extends until the merging point where the jets merge completely.
– The second zone is the merging region in which the jets are mixed and interact strongly. This area is quickly reached in the case of non-ventilated jets (Masters [17]). The velocity and temperature profiles are characterized by several maxima and minima. This zone ends is reached when the maximum velocity profile is located along the central jet axis.
– The third zone called developed region is located downstream of the combining point from which the combined jets recovers the single free jet behavior.

For the case of ventilated jets, there is an additional flow which penetrates at weak velocity between the neighboring jets breaking the vortices observed in the case of non-ventilated jets (Elbanna et al. [6]). Murai et al. [18] and Lin and Sheu [16] compared these two types of flow configurations. In the vicinity of the nozzle, the authors noted that the decrease of the velocity and the spreading for the non-ventilated jets are rapidly attained before than that of the ventilated case. In the far field of the flow, they note that there is a little difference between the two cases. The second parameter to be defined before the design of the experimental setup is the number of jets and their arrangement in space. In the case of slot jets, Pani and Dash [15] showed that the rate of decrease of the average velocity along the central jet axis decreases when the number of jets augments. However, this fact becomes negligible for a greater number (more than 7) of jets. Raghunathan and Reid [5] reported that the increase of jets number induces noise reduction but has no significant effect on the momentum of the jet. The shape of the nozzle plays also a major role in the spreading of multijets. Indeed the use of plane jets (also called slot jets) is quite common in studies of multiple jets. The use of non-ventilated slot jets will lead to the development of recirculation zones which are reduced in the case of the round jets. Another major difference is due to the effect of the nozzle's shape on the velocity and concentration distributions. Indeed, in the case of axisymmetric jet, the decrease of the velocity depends on the dimensionless streamwise abscissa axis (x/a) but in the case of the slot jets, this decrease follows a law depending on the shape of the nozzle (Grandmaison and Zettler [19]). Some authors use triangular nozzles (Koshigoe et al. [20]) or even elliptical (Schadow et al. [21]) in order to improve the mixing of the jet with the surrounding flow. Krothapalli et al. [4] measured the averaged velocity and Reynolds stresses for the configuration of the parallel rectangular jets. Laurence [22] studied the noise of a rectangular configuration of four jets. For a given spacing between the jets, it is still possible to modify the behavior of the jets mixing by inclining the injectors. Becker and Booth [23] studied the effect of the inclination of two round jets. They confirm that, in the first region of the flow, for the inclination between 15° and 45°, the jets will combine toward each other. After the merging point, they noted a faster merging jets for large angles and in the far field they have found the values expected in the case of the single jet. Others applications of multijet interaction in engineering are discussed by Q. Cao et al. [24], D. Tenchine et al. [25] and K. Svensson et al. [26]. Turbulent incompressible three jets flows are studied by Sforza et al. [27], Tanaka and Nakata [1], Krothapalli et al. [4] and Quinn [28]. These studies give much information for this type of flow interaction. Tanaka and Nakata found three flow regimes (A, B and C) depending on the ratio of the side jet to the central jet velocities. The dynamical and geometrical parameters are selected according to available data in [1] for the comparisons. This study complements the work of Tanaka and Nakata [1] by considering several velocity ratios values λ and heat transfer.

2. METHODOLOGY

2.1. Motion Equations

The fluid (air) is incompressible with constant thermo physical properties. The unsteady averaged equations which define this flow translate from the principles of conservation of the mass (eq. 1), momentum (eq. 2) and energy (eq. 3), coupled with the equations of the turbulence model:

$$\frac{\partial U_j}{\partial x_j} = 0 \tag{1}$$

$$\frac{\partial U_i}{\partial t} + U_j \frac{\partial U_i}{\partial x_j} = -\frac{1}{2}\frac{\partial P}{\partial x_i} + \frac{\partial}{\partial x_j}\left[v\frac{\partial U_i}{\partial x_j} - \overline{u_i u_j} \right] \tag{2}$$

$$\frac{\partial T}{\partial t} + \rho U_i \frac{\partial T}{\partial x_i} = \frac{\partial}{\partial x_i}\left(\frac{\mu}{p_r}\frac{\partial T}{\partial x_i} - \rho\overline{u_i\theta} \right) \tag{3}$$

Four one-point closure models are checked in this study: the standard k-ε model, the RNG k-ε model, the SST k-ω model and the RSM second order model. The standard k-ε model of Jones and Launder [29] based on the concept of Prandtl-Kolmogorov's turbulent viscosity is utilized in its high Reynolds number form. After that, Yakhot and Orszag [30] derived from the standard k-ε model, the RNG k-ε model by using the Renormalisation group (RNG) methods. Menter [31] developed a new turbulence model based on two-equation eddy-viscosity turbulence models: The shear stress transport k-ω model (SST k-ω model). The technique of the SST model is to use a k-ω formulation in the inner parts of the boundary layer and the k-ε model in the outer part of the boundary layer. To combine these two models, the standard k-ε model equations are transformed into equations based on k and ω, which leads to the introduction of a cross-diffusion term in dissipation rate equation (Menter [32] and Wilcox [33]). Reynolds Stress turbulence second order model is based on transport equations for all components of the Reynolds stress tensor and the dissipation rate. It doesn't require the eddy viscosity hypothesis (Launder et al. [34]). A preliminary study shows that both SST k-ω model and RSM model achieves the best predictions than the others models for the present configuration.

2.2. NUMERICAL PROCEDURE

This study is performed by ANSY 14.0 Fluent CFD code, using the finite volume method. This numerical method requires a transformation of all equations in conservative from (Patankar, [35]) to convection, diffusion and source terms. The boundary conditions are sketched in Fig. 1:

The ratio of the side jet to the central jet velocities is defined by $\lambda(\lambda = U_{0s}/U_{0c})$. The maximum Reynolds number of the side or the central one, $Re = U_0 a/\nu$, is fixed at 18800. At each jet exit (FG, ED, and CB) all variables are assumed constant. The inlet boundary conditions are as follow:

$$\text{Side jet (BC et FG): } U_{0s},\ V = 0,\ I_0 = k_{0s}/U_{0s}^2,\quad \varepsilon_{0s} = C_\mu \frac{(k_{0s})^{3/2}}{l_m},\ \omega_{0s} = \frac{1}{c_\mu}\frac{\varepsilon_{0s}}{k_{0s}},\ T_H \tag{4}$$

$$\text{Central jet (DE) } U_{0c},\ V = 0,\ I_0 = k_{0c}/U_{0c}^2,\quad \varepsilon_{0c} = C_\mu \frac{(k_{0c})^{3/2}}{l_m},\ \omega_{0c} = \frac{1}{c_\mu}\frac{\varepsilon_{0c}}{k_{0c}},\ T_C \tag{5}$$

where l_m is the turbulent length scale and $C_\mu = 0.09$.

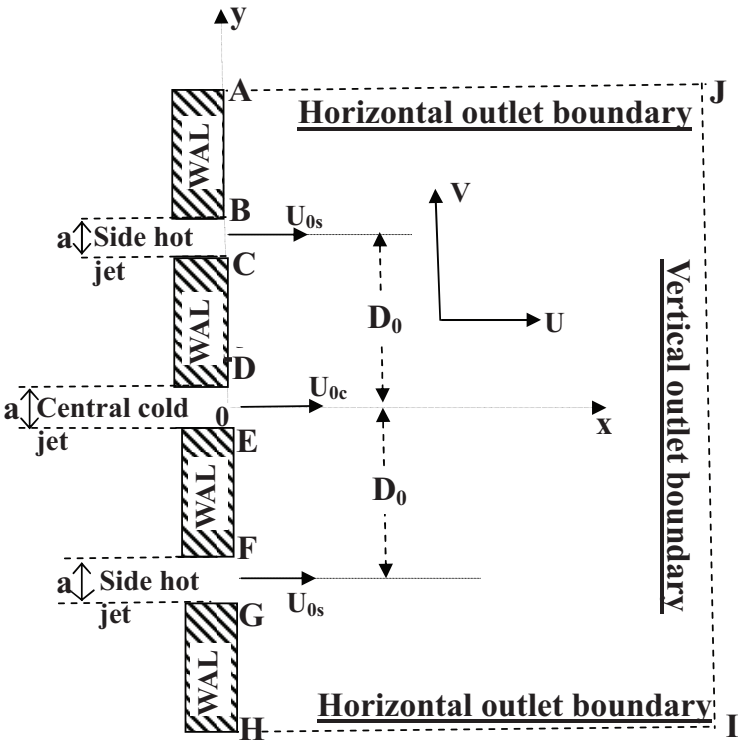

Figure 1. Geometry and boundary conditions.

– At the walls (HG, FE, DC and BA) the averaged velocity components (U, V), kinetic energy (k), dissipation (ε) and Reynolds stresses ($\overline{u_i u_j}$) are set to zero. The specific dissipation rate (ω) is kept to the asymptotic value proposed by Wilcox [33]. For the temperature, the walls are assumed adiabatic.
– At the free boundaries (IJ, HI and AJ), the static pressure and temperature are kept at atmospheric pressure and ambient temperature respectively. The free boundaries are far from the flow interaction in order to minimise their influences.

The convection and diffusion terms are interpolated using the POWER LAW scheme for each variable (Φ=V, k, T, $\overline{u_i u_j}$ ε or ω) and the SECOND ORDER scheme is applied for pressure. The pressure velocity coupling is achieved by SIMPLE algorithm. The solution is supposed converged when the normalized residues of each variable are less than 10^{-7}. The source terms are linearized to ensure the stability of the solution.

Two-dimensional structural non-uniform grids are generated (Fig. 2). The meshes are refined near the wall where high gradients prevail. The influence of the grid distribution evidenced by the neighbouring region of the jets is deepened. Several meshes are tested, only results obtained by three grids and for the case of λ = 0.602 using SST k-ω model are presented in this paper. Thus, around the jets exit, Fig. 3 (a) and (b) show that the streamwise velocity U is close to the experimental data given by in [1]). The choice fell on the mesh 2, which gives the best results. This grid distribution is used in all following calculations based on the SST k-ω model, because the geometrical parameters of this study are not modified in this work. For the other turbulence models, others grids test are investigated. For unsteady computations, several time steps are also tested. Firstly URANS simulations are performed to detect the flow regime. As shows in Fig. 4, the flow may be unsteady or steady according to the value of velocity ratio λ. In this work only steady interaction are considered. The unsteady interaction are obtained for λ = 1.10~1.20 (see ref. [1]).

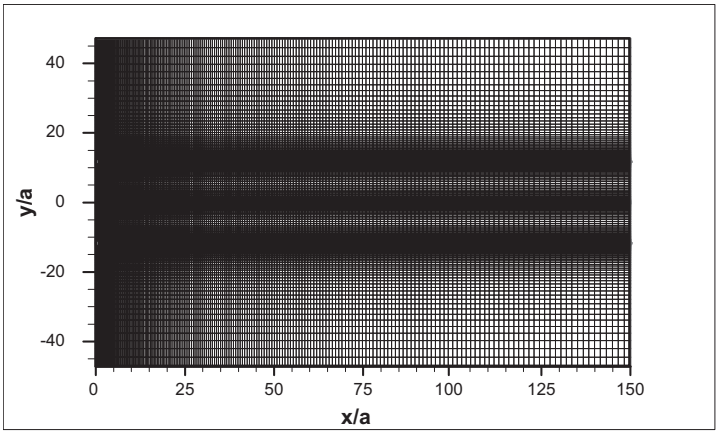

Figure 2. Typical grid.

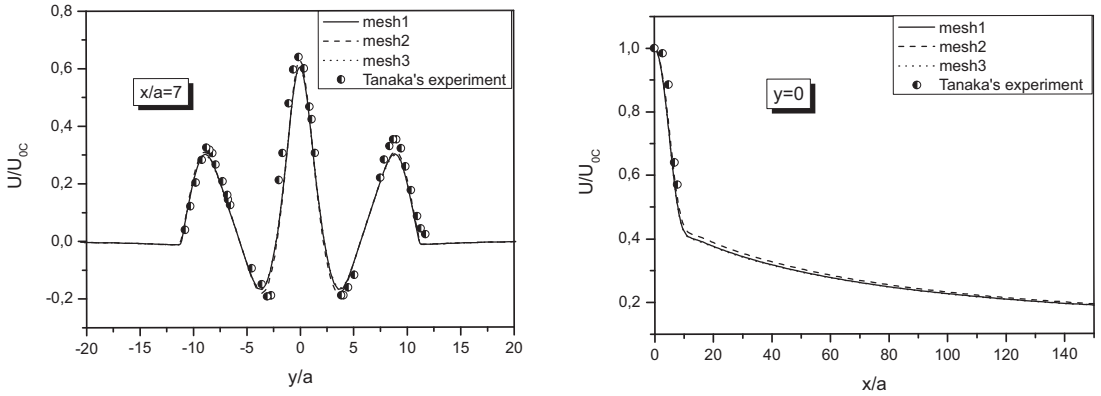

Figure 3. Influence of the grid density on the RANS results (λ = 0.602) (mesh 1 = 36300 cells, mesh 2 = 42000 cells et mesh 3 = 55000 cells).

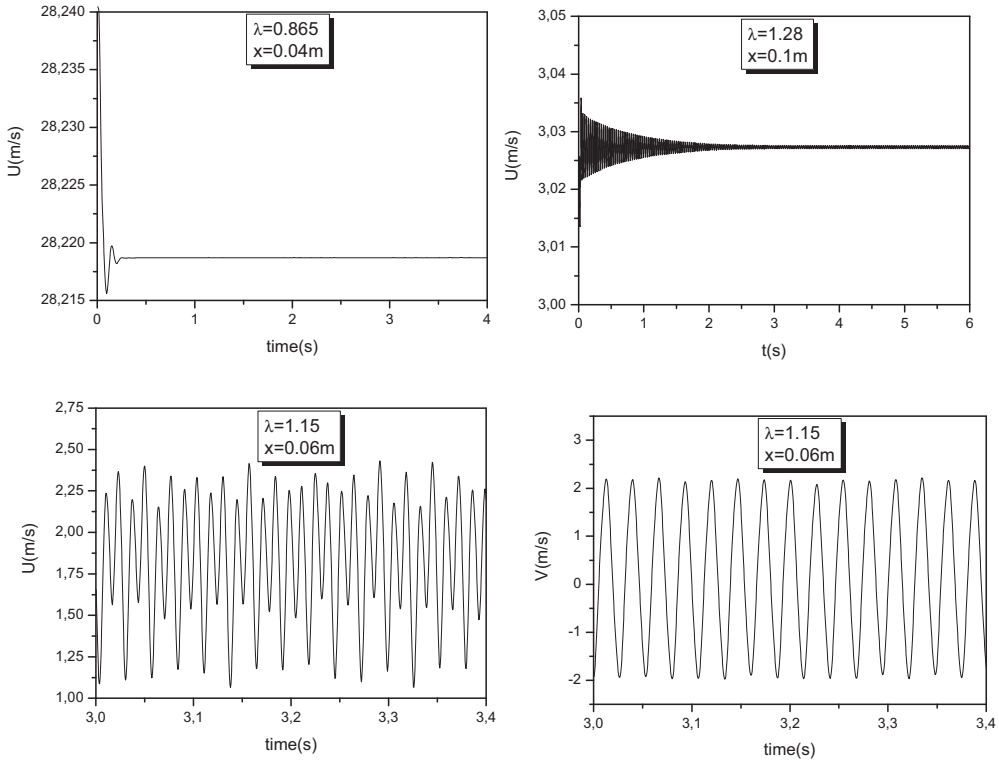

Figure 4. Time history of instantaneous velocity components at y = 0 m.

3. RESULTS AND DISCUSSION

This work describes the behaviour of the interaction of three parallel jets. Both velocity and temperature fields are investigated. The experimental work found in the scientific literature which has examined a large range of velocity ratio is that of Tanaka and Nakata [1]. As well, it seems natural to pick as reference this experimental work for the validation. The width of the nozzle of each jets is of 7 mm (a = 7 mm) and the distance between two neighbouring jets axis is D_0 (D_0 =11a). For the thermal study, the heated side jets are set at T_H and the cold central jet is kept at ambient temperature T_C = 300K.

3.1. Averaged Velocity

As mentioned above, the numerical predictions are compared with experimental available data for several velocity ratios. Fig. 5 illustrates the comparison of several turbulence models for λ=1.28. Eight cross sections are selected. The results obtained by both RSM model and SST k-ω model provide almost the same results close to the experiments data of Tanaka and Nakata [1], while the k-ε model and the RNG k-ε model underestimate slightly the experimental values. The computations using the SST k-ω model predict the averaged velocity with the best of accuracy (Fig. 5). These discrepancies are slightly more pronounced in the areas of reverse flow, which can be explained by hot-wire technique that is not suitable for recirculating flow. Unlike the flow of type A, the flows of type B and C (λ increases) will delay the merger jets, reduce the velocity of the central jet and increases those of the side jets. The one point closure SST k-ω model is used in the following calculations to save computational time, since it gives almost the same results as the RSM model.

3.2. Averaged Flow Structure

Tanaka and Nakata [1] studied the effect of the velocity ratio λ on the interference region by the detailed measures of the flow field variables. They observed three steady regimes of flow depending on the velocity ratio λ. Each flow pattern type is evidenced by visualisation picture achieved by an oil film method [1]. A good agreement is obtained with the streamlines contours (Fig. 6) and the location of stagnation points (table 1) computed on the basis of k-ω SST model. Four types of steady flow pattern are highlighted in this study.

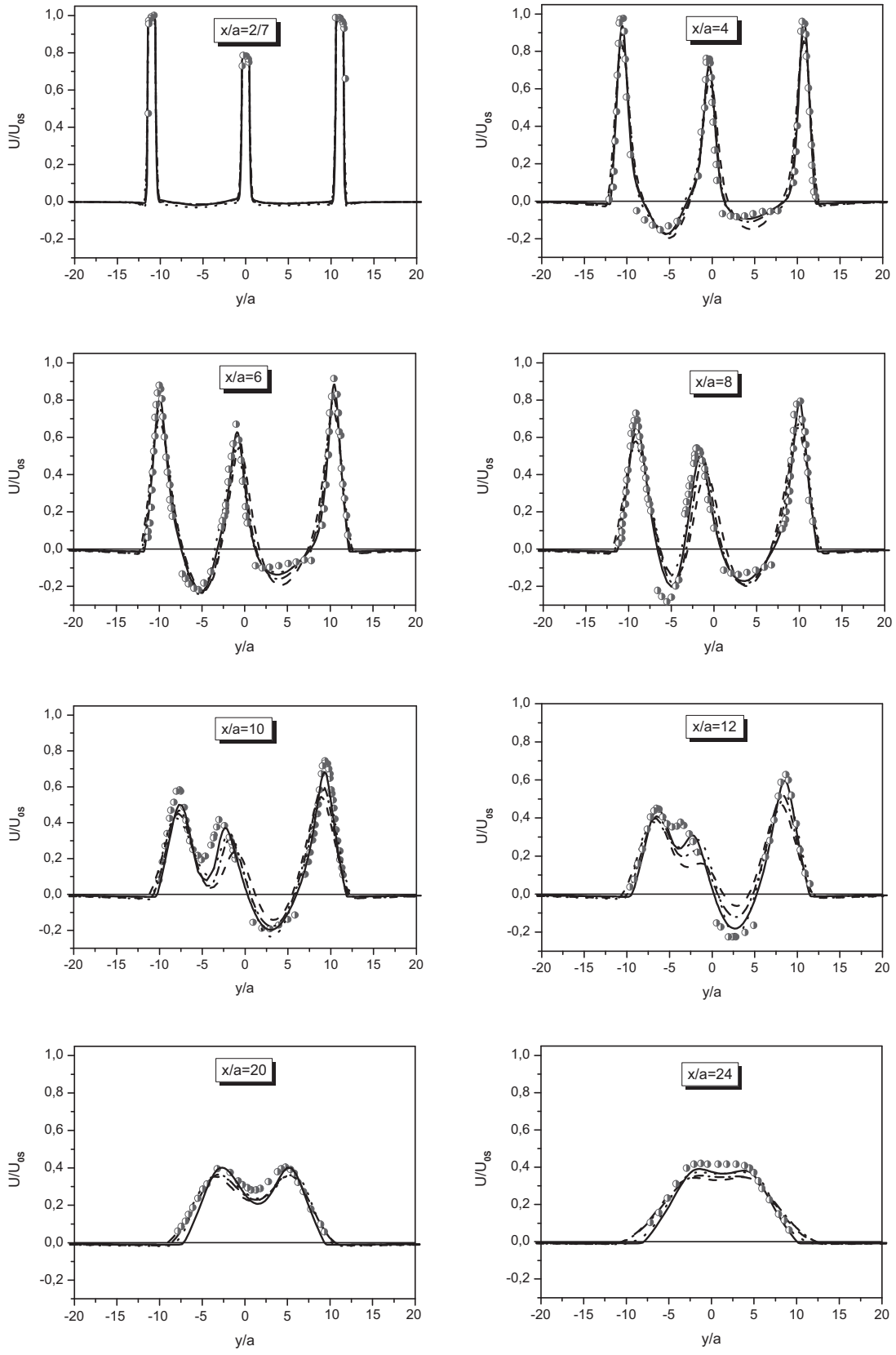

Figure 5. Turbulence model validation: normalised averaged velocity (λ = 1.28).

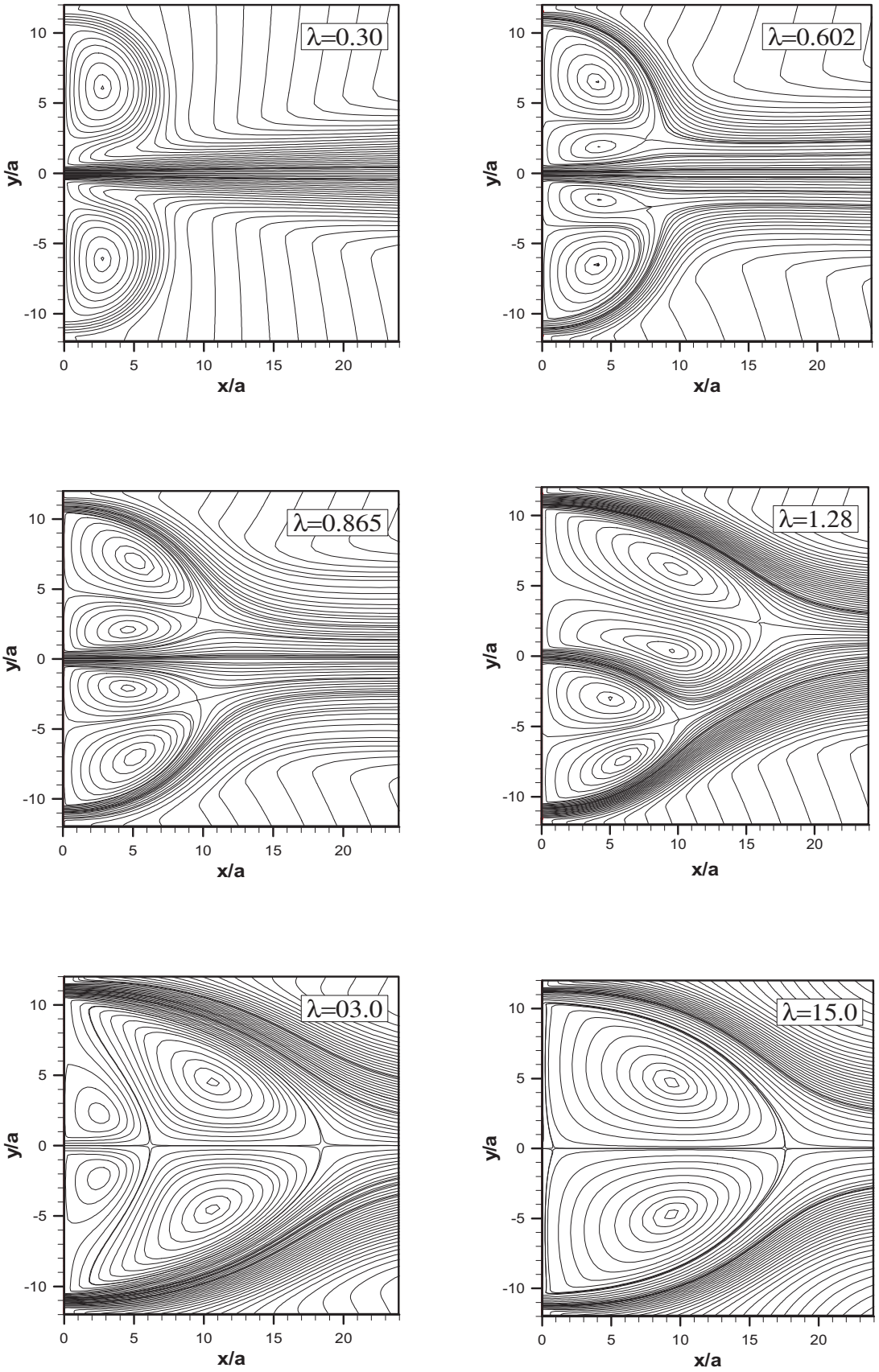

Figure 6. Computed streamlines contours (k-ω SST model).

Table 1. Stagnation points (λ=1.28)

	Stagnation Points	X_s/a Upper	X_s/a Lower
Present study	k-ω SST	16.75	9.90
	RSM	15.17	8.94
	k-ε RNG	14.49	9.70
	k-ε	13.34	9.66
Experiment	*TANAKA E. et al. [1]*	18.70	9.89

***The type A* (λ < 0.707)**

The central jet is more dominant, thus the side jets are driven and absorbed toward the central jet edges. The maximum velocity is located along the central jet axis. Two ranges of λ characterise this type of interaction:

– For 0.395 ≤λ<0.707, two secondary eddies appear between the two main recirculation zones. Two symmetrical stagnation points, on each side of the central jet axis, characterise this range of λ.

– For λ<0.395 no stagnation point is observed, the secondary vortices disappear, because the momentum of the central jet exceeds that of the side one, therefore it completely absorbs the side jets.

***The type B* (0.71 ≤ λ < 1.10)**

The recirculation zones are composed of two symmetrical counter-rotating vortices. The central jet is sucked out by the side jets. The maximum velocity is located along the central jet axis. On each side of the central jet axis, two symmetrical stagnation points are observed.

***The type C* (1.2 < λ ≤ 2.3)**

With increasing the velocity of the side jets, the recirculation zones composition become difficult to define. The central jet is rapidly deviated to one side of one lateral jet, where the first stagnation point occurs downstream. This combined flow joined the second lateral jet at the second stagnation point. The flow is highly asymmetric and merging jets is slower as in the preceding case. The maximum velocity is not located along the central jet axis.

It also should be noted that at the transition between this cases and the previous case, the central jet oscillates between the two side jets which generates some very noisy configurations and unsteady behavior (Tanaka and Nakata [1], Salantey [13]).

***Type D* (2.3<λ<20)**

For λ = 15, a reversed flow occurs in the central region of two outside jets before combining and completely overcomes the central jet and the first stagnation point is pushed back upstream. Unlike the previous case, it should be pointed that the structure of the flow becomes symmetric and the two stagnation points are situated on the central jet axis Fig. 6 (λ = 3). The structure of the plane parallel dual jet flow (Fig. 6) is obtained progressively with the increase of λ: This is a phase of slow transition to the two jets flow.

The analysis of streamlines allows to propose a new classification which is shown schematically in Fig. 7:

– The type A is characterized by no stagnation point (λ < 0.395). The schematic representation of this type of interaction has been more detailed than that of Tanaka and Nakata [1].

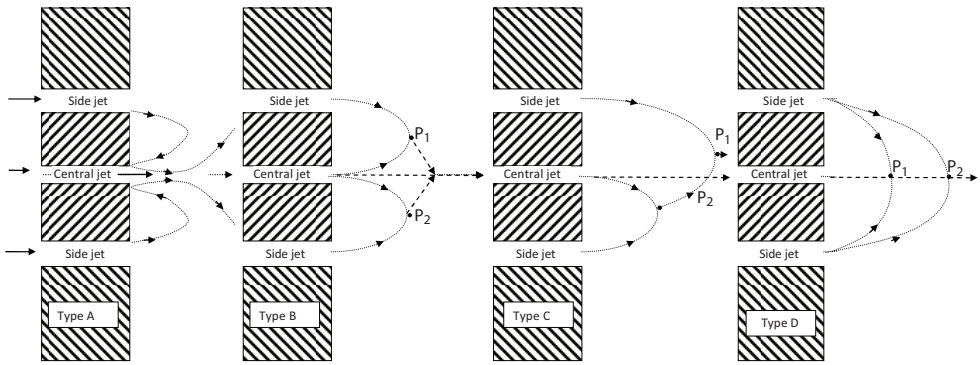

Figure 7. New flow patterns classification.

– The type B are characterized by two stagnation points (P1, P2) located symmetrically to the axis of the central jet.
– The type C is characterized by two stagnation points (P1, P2) located asymmetrically to the central jet axis.

The type D is characterized by two stagnation points (P1, P2) located on the central jet axis.

For the validation, a test case of λ=1.28 is presented in Table1. Fig. 6 evidences the displacement of the stagnation points by the flow pattern type. It is found that the best results are those of the k-ω SST model. The study of Tanaka and Nakata [1] is conducted using both hot wire and Pitot tube which are subject to serious errors (Nasr and Lai [8]).

In order to analyze the influence of the velocity ratio on the flow structure, vorticity contours are plotted. The vortical structure of the three jets interaction for several velocity ratios is illustrated in Fig. 8. As it can be seen, the shear layers development of each jet induces the penetration of the side jet in the central jet shear layers. The maximum value of vorticity magnitude is obtained in the shear layers that compose each jet, which becomes more significant for type C flow pattern.

The analysis of the Fig. 9 shows that the presence of the hot fluid from the side jets is highlight by the maxima of the isotherms in the vicinity of the nozzles. The dispersion of the temperature is controlled by the vortices (Fig. 6). The isotherms follow the behavior of the streamlines contours at the outlet and in the vicinity of the nozzles. One notices a slower turbulent heat diffusion for small values of λ. Symmetrical contours are obtained for each velocity ratio excepting the case λ = 1.28. The forced convective phenomena are highlighted by the heating flow of the side jets.

3.3. Developed region

In the fully developed flow region, after the merging point, the structure of single jet flow happens. It is known that the distributions of the averaged *x*-component velocity U(y) at x/a = 128 (Fig. 10(a)), has the same shape for each velocity ratio. At each cross-section, the maximum velocity value U_m and the half width $y_{0.5}$ of the jet are used to plot dimensionless profile ($U/U_m = f(y/y_{0.5})$). The velocity distributions for λ = 0.3, 0.602 and 0.865 fall on one common curve with that of a single jet, see Fig. 10(b). The profiles also showed a symmetrical velocity with respect to the central jet axis. The highest velocity is situated on the central axis of the centre jet. The present results follow the Gaussian curve in that they match the Goertler [36] profile in the inner part of the flow and the Tollmien [37] curve in the outer part of the flow, up to a position around ±1.5 in the dimensionless abscissa axis, when the plots begin to separate. An important point to note is that all the present computations lie between the two theoretical curves. At λ = 1.28, the Fig. 10(a) and (b) showed that the symmetrical pattern is broken for the jet and, as a consequence, the point of maximum velocity will deviate from the central jet axis. It was also found that the additional jets on each side of the central jet imply its compression transversely. Therefore, the spreading of the jet of types C is less than that of the single jet (Fig. 10(b)).

3.3.1. Centerline Evolution

Pani and Dash [15] showed, in the case of slot jets, that the decay rate of the averaged velocity along the central jet decreases when increasing the number of jets. Fig. 11 (a) and (b) showed, in comparison with a single jet, that the rate of decrease of the averaged velocity along the central jet will increase as the flow is of type A (λ < 0.395) and decreases in the other flow types. In the case of the interaction of the three jets, one notes that the decay rate also depends on the type of flow. In the near-wall region, the crosswise component of the velocity along the central axis is zero except for λ = 1.28 which reflects the asymmetry of the configuration (Fig. 12(a)). Fig. 12(b) shows the centerline pressure coefficient ($P/0.5\rho U_0^2$) for the jets, the single jet shows a shorter core length relative to the multijet configuration. The main reason behind this being that the interaction between neighboring jets occur at some downstream distance where centerline pressure shows an increase in value. This results in shocks due to a lesser mixing with the ambient air because of the presence of the neighboring jets. The centerline pressure shows a similar decrease to that of the single jet decay. The centerline pressure near the jets exit shows an increase which reaches a maximum indicating complete interaction/merging of the multiple jets. The farther downstream is the point of maximum centerline pressure from the nozzle exit plane, the lesser is the mixing process occurring in jets. The location of maximum centreline pressure moves downstream because the increased velocity ratio λ between the jets shifts the merge point further downstream (the merger of jets is more downstream as discussed previously). Pressure curve shows the

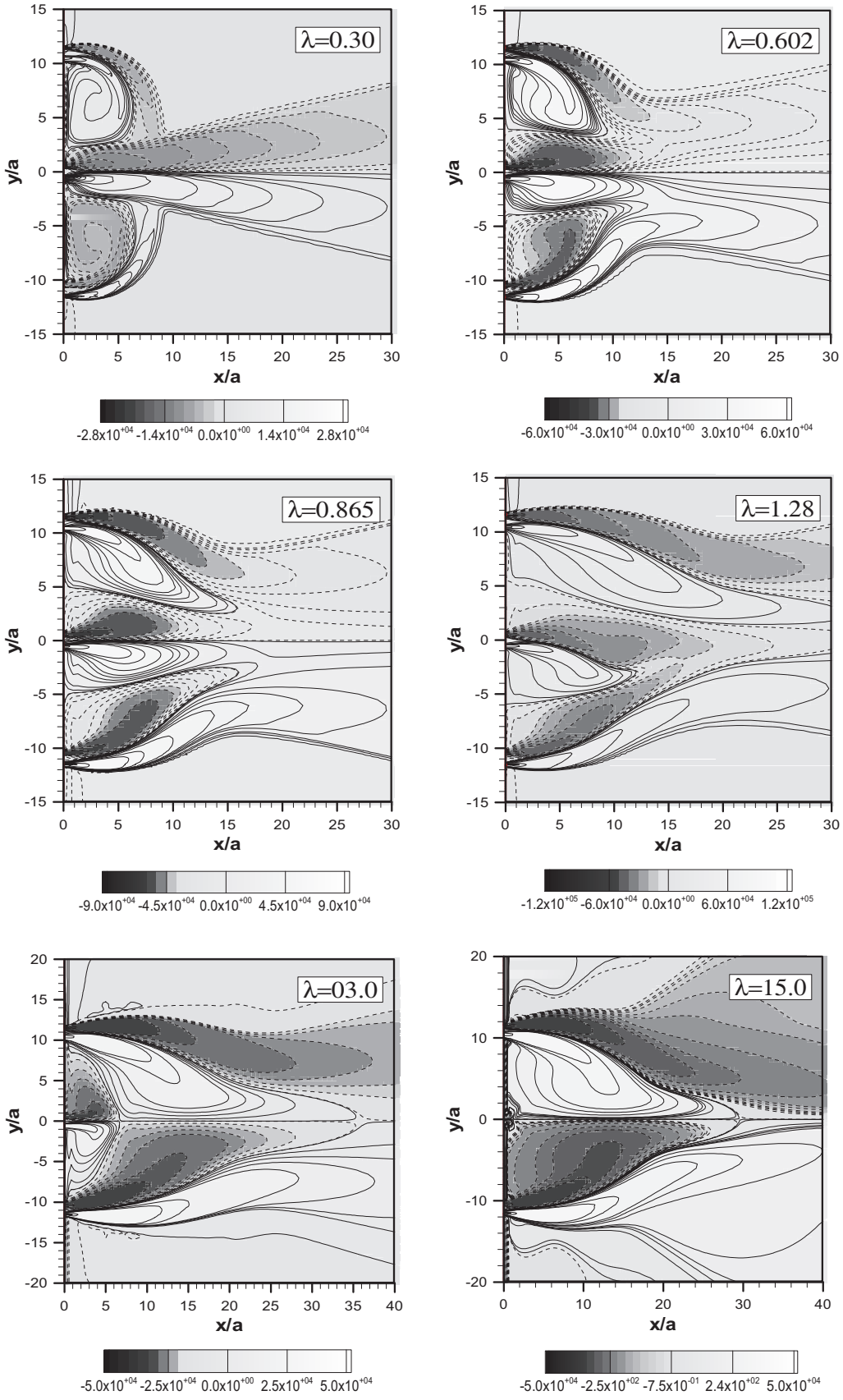

Figure 8. Vorticity contours (in s^{-1}).

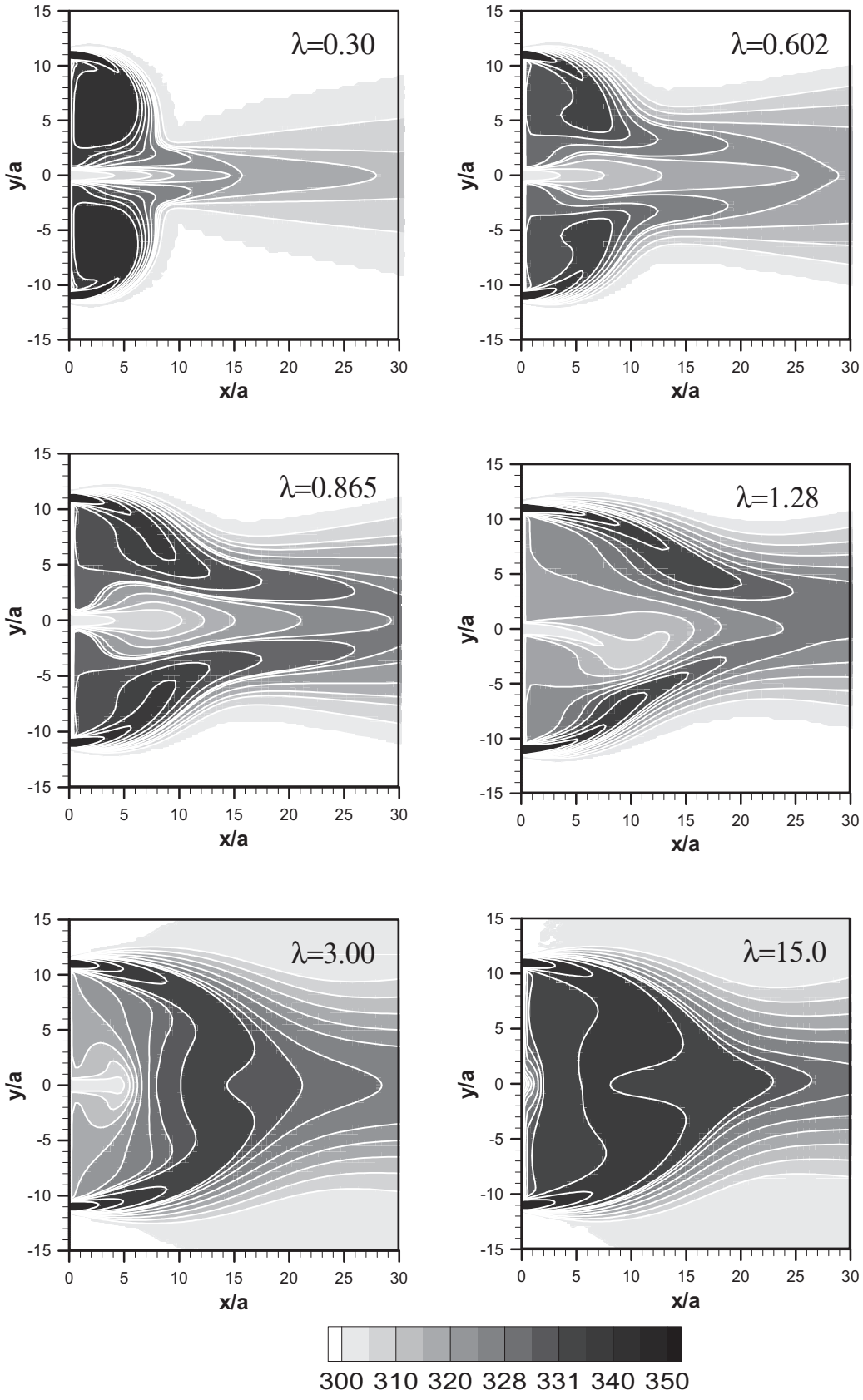

Figure 9. Averaged temperature (in K) contours for different λ for 10°C ≤ Δ T ≤ 50°C.

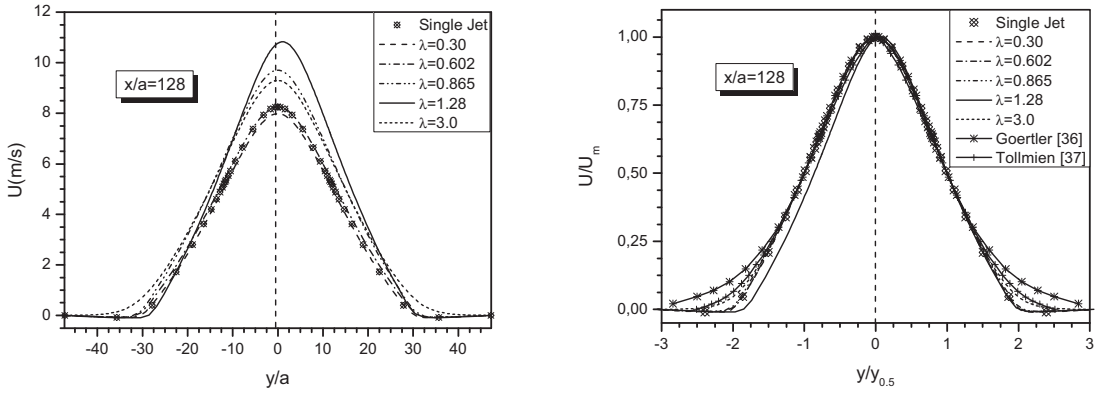

(a) (b)

Figure 10. Cross-streamwise profiles of the averaged velocity U.

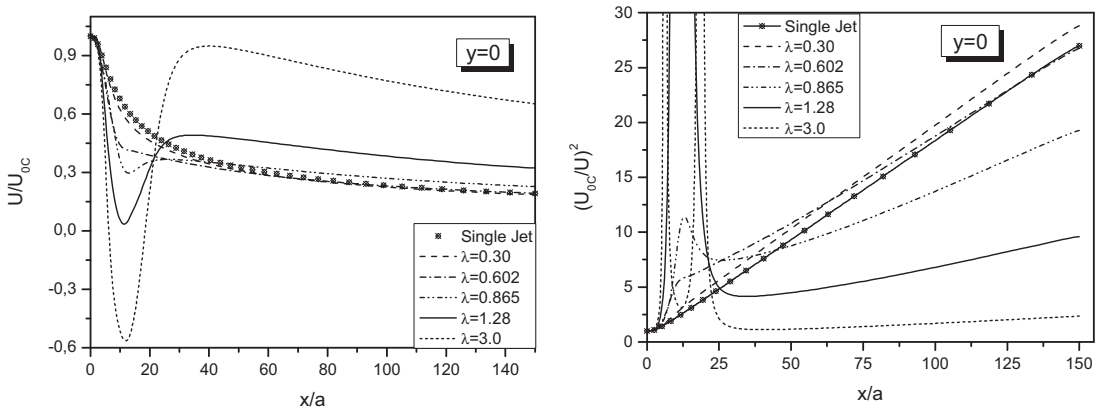

(a) (b)

Figure 11. Decay of centreline velocity.

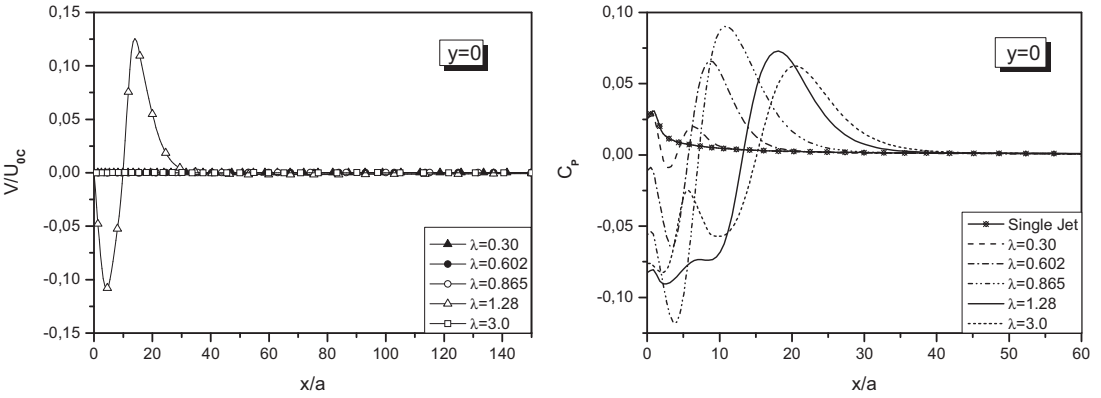

(a) Crosswise velocity (b) Pressure coefficient

Figure 12. Centreline evolution.

existence of two maxima (λ = 1.28) with reference to the first merger of the central jet with one of the side jets and to the second merger of the combined jets with the remainder side jet, the second merger leads to greater mixing. We note only one minimum value for the interactions of type A and type B and two minimum values for the cases of Type C and Type D corresponding to the location of the centres of vortices. Type C and Type D flow patterns confirm the displacement of the side eddies relative to the secondary eddies (see Fig. 6).

3.3.2. Side Jet Axis Evolution

Similarly as the centerline velocity evolution, the distribution of the velocity components and pressure are plotted along each side jets axis ($y = \pm D_0$). These figures give some information on the behavior of this type of flow interaction far from the central jet axis (Fig. 13). The x-velocity distribution along of each side jet axis are superposed ($U_{up} = U_{down}$) for $\lambda \neq 1.28$, confirming the perfect symmetry of the flow pattern. But the case $\lambda = 1.28$ presents two different distributions ($U_{up} \neq U_{down}$) corresponding to the asymmetrical configuration Fig. 13(a)). For each jet side axis, the y-velocity are opposite for the symmetrical cases ($V_{up} = -V_{down}$). They are different ($V_{up} \neq -V_{down}$) for the asymmetrical interaction

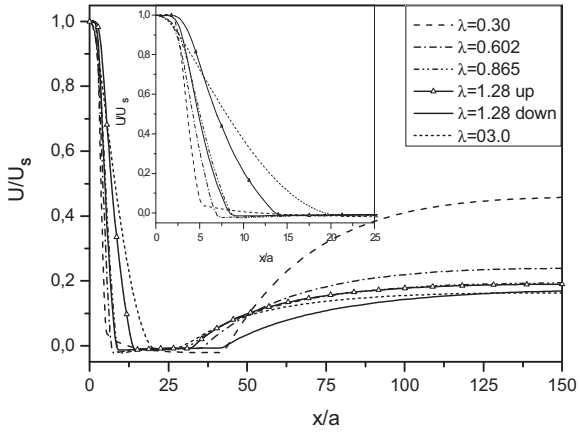

(a) Averaged streamwise velocity

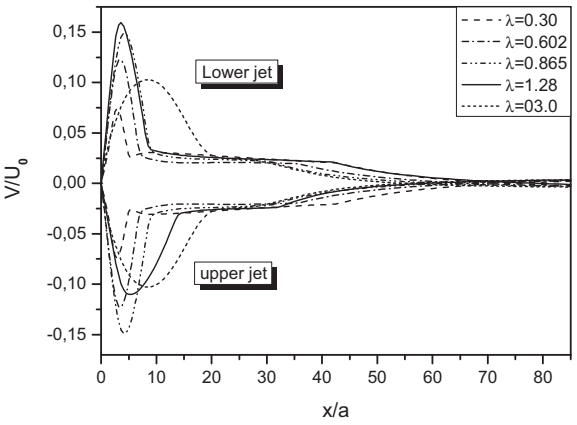

(b) Averaged crosswise velocity

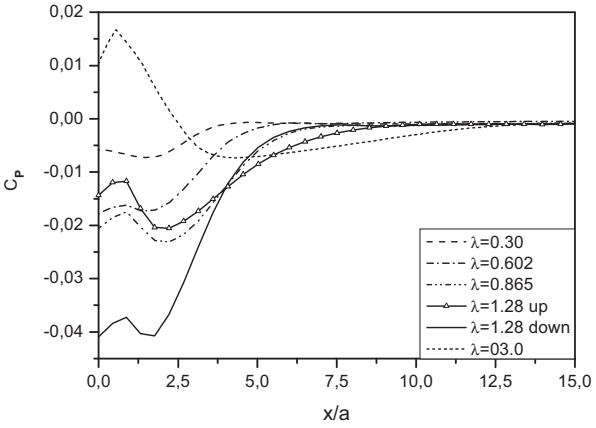

(c) Centreline pressure coefficient

Figure 13. Side jet axis evolution.

(Fig. 13(b)). The pressure coefficient has the same behavior than the x-velocity component, ie: $P_{up} \neq P_{down}$ for the asymmetrical interaction and $P_{up} = P_{down}$ for the symmetrical interaction (Fig. 13(c)). One notes that the strong depressions of the central jet and that of the lower side jet, push them to join the upper side jet in two steps.

3.4. Temperature Field

The purpose of this paper is about the heat transfer process by jets. One considers a cold central jet between two hot side jets, for several velocity ratios. Several temperature differences between the hot jet and the cold jet ($10°C \leq \Delta T \leq 50°C$) are considered. As discussed previously, the isotherms are similar for each temperature difference. The cold jet propagates between the two hot side jets except for the flow of type D where the cold jet is entirely encircled by the hot jets (Fig. 9).

3.4.1. Temperature Evolution in Fully Developed Region

Fig. 14(a) and (b) shows the predicted temperature profiles in the self-similar zone as resulting from the different values of λ. These simulating curves match very closely the Ramaprian et al. [38] experimental data in the inner part of the flow; the plots begin to separate up to a position around ±1.5 in the dimensionless abscissa axis. However, the temperature curve of the type D ($\lambda = 3$) is superposed to the Ramaprian et al. ([38] profile. For purposes of comparison, Figs. 10(b) and 14(b) show that the calculated curves for the dimensionless velocity and dimensionless temperature at the same cross section coincide. The normalized temperature profiles are similar for several ΔT. Therefore, the temperature spreading of the jet of types (A, B and C) is less than that of the single jet (Fig. 14(b)). Furthermore, the temperature spreading of the type C pattern is the smallest one. At $\lambda = 1.28$, the Figs. 14(a) and (b) shows asymmetrical pattern for the jet and, consequently, the point of maximum temperature will deviate from the central jet axis.

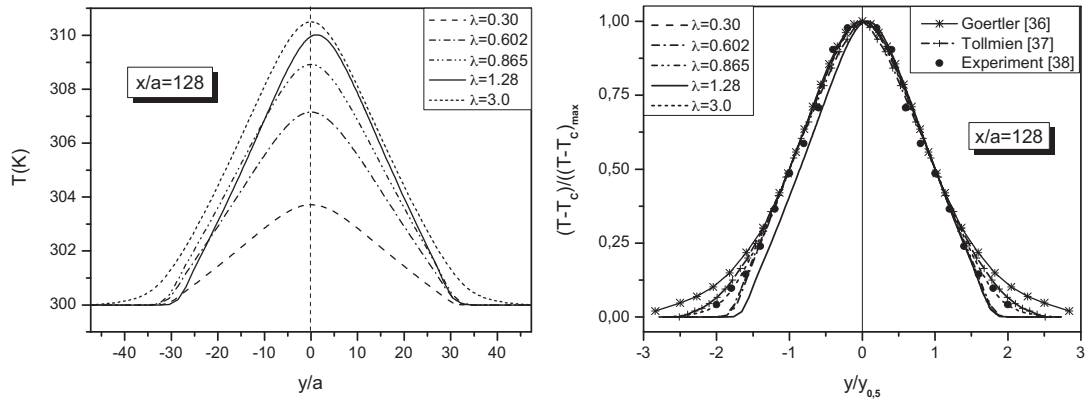

(a) Averaged temperature for ΔT=30°C

(b) Self-similarity profiles

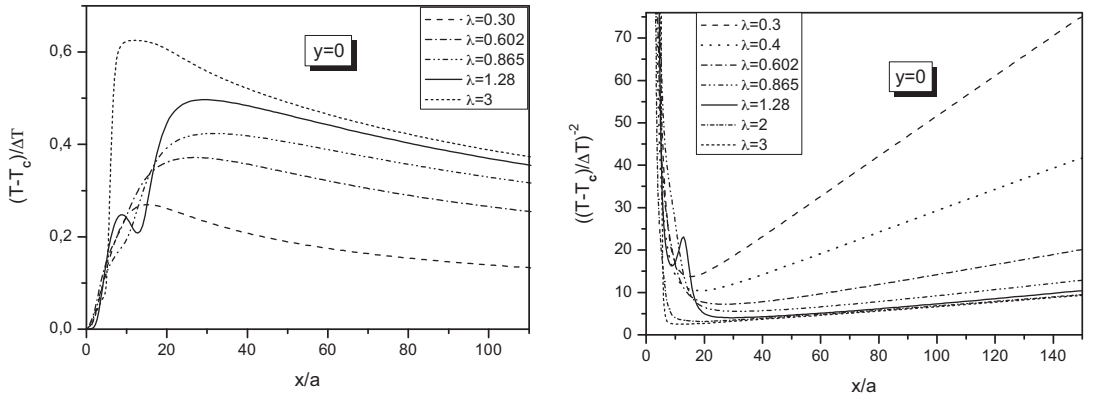

(c) Centreline temperature evolution

(d) Centreline temperature decay

Figure 14. Temperature evolution for $10°C \leq \Delta T \leq 50°C$.

3.4.2. Centerline Temperature Evolution

The influence of the velocity ratios is illustrated in Fig. 14(c) which shows the dimensionless increment of temperature at the jet centerline versus the dimensionless streamwise coordinate x/a. The parameter $\Delta\Theta$ ($\Delta\Theta = (T - T_C)/(T_H - T_C)$) is the increment of temperature at the jet centerline due to the interaction of hot side jets with the central cold jet as compared to the temperature at the centerline of the coldest jet (see Fig. 14(c)). As the velocity ratios increases, the maximum temperature at the jet centerline increases and is shifted upstream for types C and D of flow: This implies that the diffusion of heat is faster when λ increases. As the velocity ratios increases, the maximum temperature at the jet centerline increases and is shifted downstream for types A and B of flow: This can be explained by slower diffusion of heat when λ decreases. For $\lambda = 1.28$, the distorted curve with two maximum values corresponding to the first and second mixing respectively. Fig. 14(d) shows that the rate of decrease of the averaged temperature along the central jet will increase as the velocity ratio λ decreased.

4. CONCLUSION

The flow patterns in the three parallel jets change with the variation of the nozzle velocity jet exit ratio ($\lambda = U_{0S}/U_{0C}$). Four URANS models are tested for several λ. The velocity ratio plays a major role in the flow time evolution.

In comparison with the experiment, the SST k-ω model and RSM model results are better than those of the standard k-ε model and RNG k-ε model.

- A new classification of the steady flow pattern is highlighted. Four types of flow are identified instead of the three cited in the literature.
- For type C, the symmetrical pattern is broken then the maximum velocity and maximum temperature is shifted from the central jet axis in the developed region. The additional jets on each side of the central jet involve the decrease of the temperature spreading of the jet in the developed region. For type C, both the velocity and temperature spreading of the jet of type C are the smallest.
- In comparison with a single jet, it was found that the addition of side jets increases the rate of decrease of the centerline velocity for the flow of type A and decreases in the other cases. Thus it appears that the velocity decay rate depends not only on the number of jets but also from the type of flow.
- The minima of the pressure coefficient curves along the central jet axis, for several values of λ, allow to locate the centres of the vortex.
- The centerline profiles of the averaged temperature are similar for different temperature gaps ($10°C \leq \Delta T \leq 50°C$) at each velocity ratios. All simulated profiles agree well with Goertler's profiles in the inner part and those of Tollmien in the outer part of the flow.
- The diffusion of temperature strongly depends on velocity ratio (λ)

The instationary behaviour will studied in the future.

NOMENCLATURE

a	Slot nozzle width [m]
Do	Distance between two nozzle [m]
x, y	Streamwise and transverse coordinate [m]
x_S	Stagnation point [m]
b	Half width of the jet (the value of y where U is equal to half the maximum velocity) [m]
$y_{0.5}$	Vertical position from the axis to the point at which the velocity is equal to $1/2U_m$
U	Averaged velocity in the x-direction [ms^{-1}]
V	Averaged velocity in the y-direction [ms^{-1}]
U_i, U_j	Velocities components [ms^{-1}]
U_0	Jet exit averaged velocity [ms^{-1}]
U_{0C}	Central jet exit velocity [ms^{-1}]
U_{0S}	Side jet exit velocity [ms^{-1}]
λ	Nozzle discharge velocity ratio
Re	Reynolds number
$\overline{u_i u_j}$	Reynolds stress component [m^2s^{-2}]

P Averaged pressure [Pa]
T Averaged temperature [K]
K Turbulent kinetic energy, [m^2s^{-2}]

Greek symbols

ω Specific dissipation rat [s^{-1}]
ε Dissipation of turbulent energy [$m^2.s^{-3}$]
ρ Density of air [Kgm^{-3}]
μ Dynamic viscosity [$Kgm^{-1}s^{-1}$]
ν Kinematic viscosity [m^2s^{-1}]
ν_t Turbulent eddy viscosity [m^2s^{-1}]
ν_e Effective viscosity [m^2s^{-1}]
ϰ Von Karman constant

Subscripts

t Turbulent
w Wall
up For y = Do
down For y = -Do
C Cold temperature
H Hot temperature

REFERENCES

[1] E. Tanaka, and S. Nakata, The interference of two-dimensional parallel jets (3rd Report,The Region near the Nozzles in Triple jets), Bulletin of the JSME, Vol. 18 N°124, October 1975, pp. 1134–1141.

[2] E. Tanaka, The interference of two dimensional parallel jets (1st Report, Experiments on Dual Jets), Bulletin of the JSME, Vol. 13 N°56, February 1970, pp. 272–280

[3] E. Tanaka, The interference of two dimensional parallel jets (2nd Report, Experiments on the combined flow of Dual Jets), Bulletin of the JSME, Vol. 17 N°109, July 1974, pp. 920–957.

[4] A. Krothapalli, D. Baganoff, and K. Karamchetti, On the mixing of a rectangular jet, Journal of Fluid Mechanics, Vol. 107, 1981, pp. 201–220.

[5] S. Raghunathan, I.M. and Reid, A study of multiple jets, AIAA Journal, Vol. 19, 1981, pp. 124–127.

[6] H. Elbanna, S. Gahin, and M.I.I. Rashed, Investigation of two plane parallel jets, AIAA Journal, Vol. 21 N°7, 1982, pp. 986–991.

[7] J.H. Jung, and G.J. Yoo, Analysis of unsteady turbulent triple jet flow with temperature difference, *Journal of Nuclear Science and Technology*, Vol. 41 N°9, September 2004, pp. 931–942.

[8] A. Nasr, and J.C.S. Lai, Comparison of flow characteristics in the near field of two parallel plane jets and an offset plane jet, Physics of fluid, Vol. 9 N°10, 1977, pp. 2919–2931

[9] N. Kimura, H. Miyakoshi, and H. Kamide, Experimental Investigation on Transfer Characteristics of Temperature Fluctuation From Liquid Sodium to Wall in Parallel Triple-Jet, *International Journal of Heat and Mass Transfer*, Vol. 50 N°9, 2007, pp. 2024–2036.

[10] A. Tokuhiro, and N. Kimura, An Experimental Investigation on Thermal Striping Mixing Phenomena of a Vertical Non-buoyant Jet with two Adjacent Buoyant Jets as measured by Ultrasound Doppler Velocimetry, Nuclear Engineering and Design, Vol. 188 N°1, 1999, pp. 49–73.

[11] K. Yamamoto, and K. Hishida, Quantitative Visualisation of turbulent mixing in parallel triple plane jets, Experimental Heat Transfer Fluid Mechanics and Thermodynamics, N°2, 2001, pp. 1029–1034.

[12] N.H. Buddhika, A Numerical Study of Heat Transfer Performance of Oscillatory Impinging Jets, International Journal of Heat and Mass Transfer, Vol. 52, 2009, pp. 396–406

[13] L. Salentey, Etude expérimentale du comportement de brûleurs à jets séparés. Application à la combustion gaz naturel-oxygène pur, PhD thesis, Faculté des Sciences et Techniques de l'Université de Rouen, 2002.

[14] C. Lesieur, Modélisation de la combustion turbulente non-prémélangée dans un brûleur à jets séparés application à la stabilisation d'une oxy-flamme., PhD thesis, Institut National des Sciences Appliquées de Rouen, 2003.

[15] B.S. Pani, and R.N. Dash, Three-dimensional single and multiple free jets, Journal of Hydraulic Engineering, ASCE, Vol. 109 N°2, 1983, pp. 254–269.

[16] Y.F. Lin and M.J. Sheu, Interaction of parallel jets, AIAA Journal, Vol. 29 N°9, 1991, pp. 1372–1373.

[17] G.F. Marsters, Interaction of two plane parallel jets, AIAA Journal, Vol. 15 N°12, January 1977, pp. 1756–1762.

[18] K. Murai, M. Taga, and K. Akagawa, An experimental Study on Confluence of Two Dimensional Jets, Bulletin JSME, Vol. 19, 1976, pp. 956–964.

[19] E.W. Grandmaison, and N.L. Zettler, Turbulent Mixing in Coflowing Plane *Jets*, The Canadian Journal of Chemical Engineering, Vol. 67 N°6, *1989*, pp. 889–897.

[20] S. Koshigoe, E. Gutmark, and K. Schadow, Initial development of non circular jets leading to axis switching, AIAA J, Vol. 27, 1989, 411–419.

[21] K.C. Schadow, E. Gutmark, S. Koshigoe, and K.J. Wilson, Combustion-related shear-flow dynamics in elliptic supersonic jets, AIAA Journal, Vol. 27 N°10, 1989, pp. 1347–1353.

[22] J.C. Laurence, Turbulence Studies of Rectangular Slotted Noise-Suppressor Nozzle, NASA TECHNICAL NOTE D-294, 1960.

[23] H.A. Becker, and B.D. Booth, AIChE J. Vol. 21 N°5 , 1975, pp. 949–958.

[24] Q. Cao, D. Lu, and J. Lv, Numerical investigation on temperature fluctuation of the parallel triple-jet, Nuclear Engineering and Design, Vol. 249, 2012, pp. 82–89.

[25] D. Tenchine, S. Vandroux, V. Barthel, and O. Cioni, Experimental and numerical studies on mixing jets for sodium cooled fast reactors, Nuclear Engineering and Design, vol. 263, 2013, pp. 263–272.

[26] K. Svensson, P. Rohdin, B. Moshfegh, and M. Tummers, Numerical and experimental investigation of the near zone flow field in an array of confluent round jets, International Journal of Heat and Fluid Flow, vol. 46, 2014, pp. 127–146.

[27] P.M. Sforza, M.H. Steiger, and N. Trentacoste, Studies on three-dimensional viscous jets, AIAA Jounal, Vol. 4 N° 5, 1966, pp. 800–806.

[28] W.R. Quinn, Turbulent Free Jet Flows Issuing from Sharp-Edged Rectangular Slots: The Influence of Slot Aspect Ratio, Experimental Thermal and Fluid Science, Vol. 5, 1992, pp. 203–215

[29] W.P. Jones, and B.E. Launder, The prediction of laminarization with a two-Equation model of turbulence. International Journal of Heat Transfer, Vol. 15, 1972, pp. 301–304.

[30] V. Yakhot, and S.A. Orszag, Renormalization Group Analysis of Turbulence. I. Basic Theory, J. Sci. Comput, Vol. 1 N°1, 1986, pp. 3–51.

[31] F.R. Menter, Zonal Two Equation k-ω Turbulence Models for Aerodynamic Flows, AIAA Journal, 1993, pp. 93–2906.

[32] F.R. Menter, Two-equation eddy-viscosity turbulence models for engineering applications, AIAA Journal, Vol. 32 N°8, 1994, pp. 1598–1605.

[33] D.C. Wilcox, Turbulence Modelling for CFD, DCW Industries Inc, La Canada, CA, 1993.

[34] B.E. Launder, G.J. Reece, and W. Rodi, Progress in the developments of a Reynolds-stress turbulence closure, J. Fluid Mechanics, Vol. 68, 1975, pp. 537–586.

[35] S.V. Patankar, Numerical heat transfer and fluid flow, Series in Computational methods in mechanics and thermal sciences, Hemisphere Publishing Corp. & Mc Graw Hill, 1980.

[36] H. Goertler, Berechnung von Aufgaben der freien Turbulenz auf Grund eines neuen Naherungsansatzes, Z.A.M.M., 22, 1942, pp. 244–254.

[37] W. Tollmien, Berechnung turbulenter Ausbreitungsvorgange. Z.A.M.M., 6, 1926, pp. 468–478. (English translation, N.A.C.A. TM, 1085, 1945)

[38] B.R. Ramaprian and M.S. Chandrasekhara, LDA Measurements in Plane Turbulent Jets, Transactions of the ASME - Journal of Fluids Engineering, Vol. 107, 1985, pp. 264–271.